

# Wide Range Fabrication of Wrinkle Patterns for Maximizing Surface Charge Density of a Triboelectric Nanogenerator

Xiaoliang Cheng, Zijian Song, Liming Miao, Hang Guo, Zongming Su, Yu Song,  
and Hai-Xia Zhang, *Senior Member, IEEE*

**Abstract**—Wrinkle patterns, as a simple surface patterning process, have been previously used in triboelectric nanogenerator (TENG) to improve electric performance. However, since lacking an effective way to control the wrinkle pattern in a wide range, the influence of wrinkle pattern to the performance of TENG has not been systematically investigated. This paper proposes a pre-heating process to adjust the modulus of uncured polydimethylsiloxane, resulting in wide-range controllable wrinkle patterns. Quantitative measurements show the wrinkle pattern wavelength ( $\lambda$ ) could be varied from 20.13 to 0.92  $\mu\text{m}$  by pre-heating time from 0 to 10 min. Using this wide-range wrinkle pattern, the performance of TENG was remarkably improved with a higher surface charge density of 537.6  $\mu\text{C}/\text{m}^2$ . Through simulating the impact of interfacial structures deformation, we found smaller structure leading to higher performance of TENG at low pressure region and smaller surface area resulting in a lower performance, which accounted for the correlation we observed in this paper, and could guide the structure design for a high-charge-density TENG. This paper provides an alternative way for controlling wrinkle pattern as well as increasing surface charge density of TENG from fabrication process, simulated results, theoretical analysis, and quantitative measurements. [2017-0154]

**Index Terms**—Wrinkle pattern, fluorocarbon plasma, triboelectric nanogenerator.

## I. INTRODUCTION

WRINKLE structures fabricated on elastic substrates such as PDMS are becoming increasingly significant, owing to their features of simple fabrication process, flexibility, stretch-ability, and the adaptation for large area pattern [1], [2]. These patterns have exhibited a wide range of applications, including optical devices [3], stretchable electronics.[4], microfluidics. [5], tunable adhesion and

wettability [6], [7], and flexible pressure sensors [8]. Typically, wrinkle patterns take place in a multilayered film comprising a stiff cover layer on a relatively soft, elastic substrate, with tunable wrinkle wavelength  $\lambda$  by adjusting the thickness of the stiff layer and the pre-strain [9]–[11]. However, applying the outer force usually requires a free-standing membrane, which would inevitably increase the thickness of this membrane and restrict their applications. Besides, there is a growing demand for developing more methods for controlling and adjusting the wrinkle patterns in wider range to enable and broaden their applicable fields.

TENG is developing to be a potential technology for energy harvesting with features of simple structure, low cost, and well-adaptation for different materials [12]–[16]. In the recent studies, it has been successfully used to harvest the energy from water [17], wind [18], human motions [19] and even heartbeat [20]. However, the electric performance of TENG still needs to be further improved to meet the requirement for traditional electronics. Considering the basic mechanism of TENG, the enhancement of surface charge density is the mostly fundamental way to get a high performance device, since both the voltage and current density are proportional to it [21]. Existing approaches for increasing the surface charge density include the utilization of micro/nano structure [22], [23], modification of surface material [24], [25], increasing of the applied force to the device [26], injection of inion charge to the surface [27], and the employment of liquid metal [28]. Among all these methods, the modification of surface material and introduce of micro/nano structure, being able to increase the ability of electron affinity and surface roughness, have been mostly employed and investigated.

Our previous work successfully combined the fluorocarbon polymer modification and surface pattern in single step using fluorocarbon plasma to treat uncured PDMS, which had significantly improved the electric performance and charge density of TENG [29]–[31]. Compared with material modification, surface pattern has larger space to be optimized to make sure a large contact area for generating more charges. Unfortunately, owing to the lack of effective methods for adjusting the wrinkle morphologies in wide range, the influence of wrinkle patterns to the electric performance of TENG hasn't been deeply investigated.

In this work, a pre-heating process is introduced for adjusting the property of uncured PDMS, leading to the formation

Manuscript received July 7, 2017; revised September 26, 2017; accepted November 25, 2017. Date of publication December 21, 2017; date of current version February 1, 2018. This work was supported in part by the National Key Research and Development Project from the Ministry of Science and Technology, China, under Grant 2016YFA0202701; in part by the National Natural Science Foundation of China under Grant 61674004, Grant 61176103, and Grant 91323304; in part by the Beijing Science and Technology Project under Grant D151100003315003; and in part by the Beijing Natural Science Foundation of China under Grant 4141002. Subject Editor R. Ghodssi. (X. Cheng and Z. Song contributed equally to this work.) (Corresponding author: Hai-Xia Zhang.)

The authors are with the Institute of Microelectronics, Peking University, Beijing 100871, China (e-mail: xlcheng@pku.edu.cn; 49620300@qq.com; maxlimit@pku.edu.cn; guohang@hust.edu.cn; szmpku@gmail.com; songyupku@pku.edu.cn; hxzhang@pku.edu.cn; ).

This paper has supplementary downloadable material available at <http://ieeexplore.ieee.org>, provided by the author.

Color versions of one or more of the figures in this paper are available online at <http://ieeexplore.ieee.org>.

Digital Object Identifier 10.1109/JMEMS.2017.2778735

of controllable wrinkle pattern. External force was applied via fluorocarbon plasma, resulting in a thinner substrate. By simply varying the pre-heating time, the wrinkle pattern wavelength successfully decreased for more than 95%. Direct observation, theoretical modeling, simulated analysis, and structural characterization were performed for comprehensive understanding of this process. Besides, the wide-range controllable wrinkle patterns were further employed to improve the electric performance of TENG, more than three times higher charge density was obtained compared with our previous results. Further analysis by electric characterization, simulation and surface area measurement shown that the dramatically decreased wrinkle pattern contributed to this improvement.

## II. EXPERIMENTAL SECTION

### A. Sample Preparation

The base solution and curing agent of commercial PDMS (Sylgard 184, Dow Corning Corporation) were mixed with a quantity ratio of 10:1. After degassed in a vacuum pump, the liquid mixture of PDMS was spin-coated onto PET/ITO film. Then it was cured immediately at 90 °C for a certain time on a hot plate and treated using an ICP etcher (Surfacings Technology Systems plc, Multiplex ICP 48443) afterwards. Finally, this sample was totally cured in an oven at 90 °C for 1 h.

### B. Surface Plasma Treatment

The fluorocarbon plasma treatment of the uncured PDMS surface was conducted using an ICP etcher (Surfacings Technology Systems plc, Multiplex ICP 48443). The RF power, platen power, gas ( $C_4F_8$ ) flow rate, and pressure were set as 0 W, 100 W, 60 sccm, 5 Pa respectively.

### C. Pattern characterization

The processed wrinkle structures with  $\lambda < 2 \mu m$  were characterized by an atomic force microscope (Dimension ICON, Bruker Corp.) in PeakForce mode, which is a featured mode of Bruker Corp. that could provide the highest resolution. Then, the results were analyzed by Nanoscope Analysis 1.5 software (Bruker Corp.). The samples with  $\lambda > 2 \mu m$  were evaluated by confocal laser scanning microscope (LEXT OLS4100, Olympus). At the same time, all the samples were photographed by an environment scanning electron microscope (ESEM, FEI Quanta 600). The error bars for wrinkle patterns were measured and calculated by three membranes from independent experiments.

### D. Quantitative Measurement System

The output voltage was measured via a digital oscilloscope (Agilent DSO-X 2014A) using a 100 M $\Omega$  probe (HP9258), and the current was amplified by a SR570 low noise current amplifier from Stanford Research systems. The upper surface was fixed to a certain place. Then a sinusoidal signal with an amplitude of 1.5 V was generated from the signal source module of the oscilloscope and amplified by an amplifier (SINOCERA YE5871A) to power the modal shaker (JZK-10),

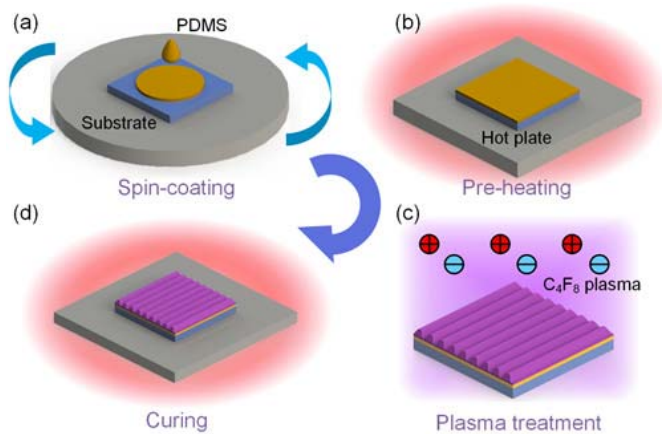


Fig. 1. Fabrication process for the wide-range wrinkle pattern. (a) Spin-coating PDMS on PET/ITO substrate. (b) Heating uncured PDMS on a hot plate. (c) Performing  $C_4F_8$  plasma treatment on pre-heated sample. (d) Curing the treated sample in an oven.

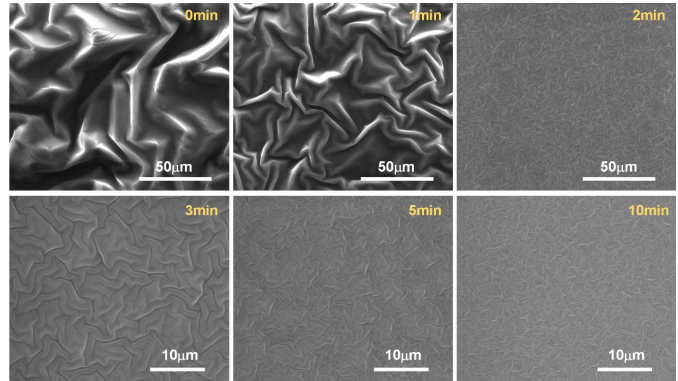


Fig. 2. SEM images of wrinkle patterns with varying pre-heating time.

which could provide a periodic and stable external force ( $\sim 50$  N) to the device. The charging ability test is measured by charging a 1  $\mu F$  capacitor under finger typing through a full-wave rectifier, while the maximum force applied to the TENG was measured to be about 50 N to make the data of this part comparable with that using the shaker. The error bars for electric performances were derived by three TENGs using membranes from independent experiments.

## III. RESULTS AND DISCUSSIONS

### A. Fabrication of Wide-Range Wrinkle Patterns

Fig. 1 diagramed the detailed fabrication process for controlling the wrinkle patterns. Firstly, prepared PDMS mixture was spin-coated onto the substrate. The sample was then heated on a hot plate within an alterable time  $t$ . Afterwards, the pre-heated membrane was treated using fluorocarbon plasma with  $C_4F_8$  gas. Finally, it was totally cured in an oven.

Following the procedure mentioned above, pattern  $\lambda$  can be easily tuned by the pre heating time  $t$ . By varying  $t$  from 0 min to 10 min, the wrinkle patterns were shown in the SEM images of Fig. 2. The wrinkle patterns exhibited dramatically decrease during  $t$  from 0 min to 2 min, while they reduced slightly from 3 min to 10 min.

To further investigate the relationship between pattern  $\lambda$  and pre-heating time  $t$ , quantitatively measurements for the

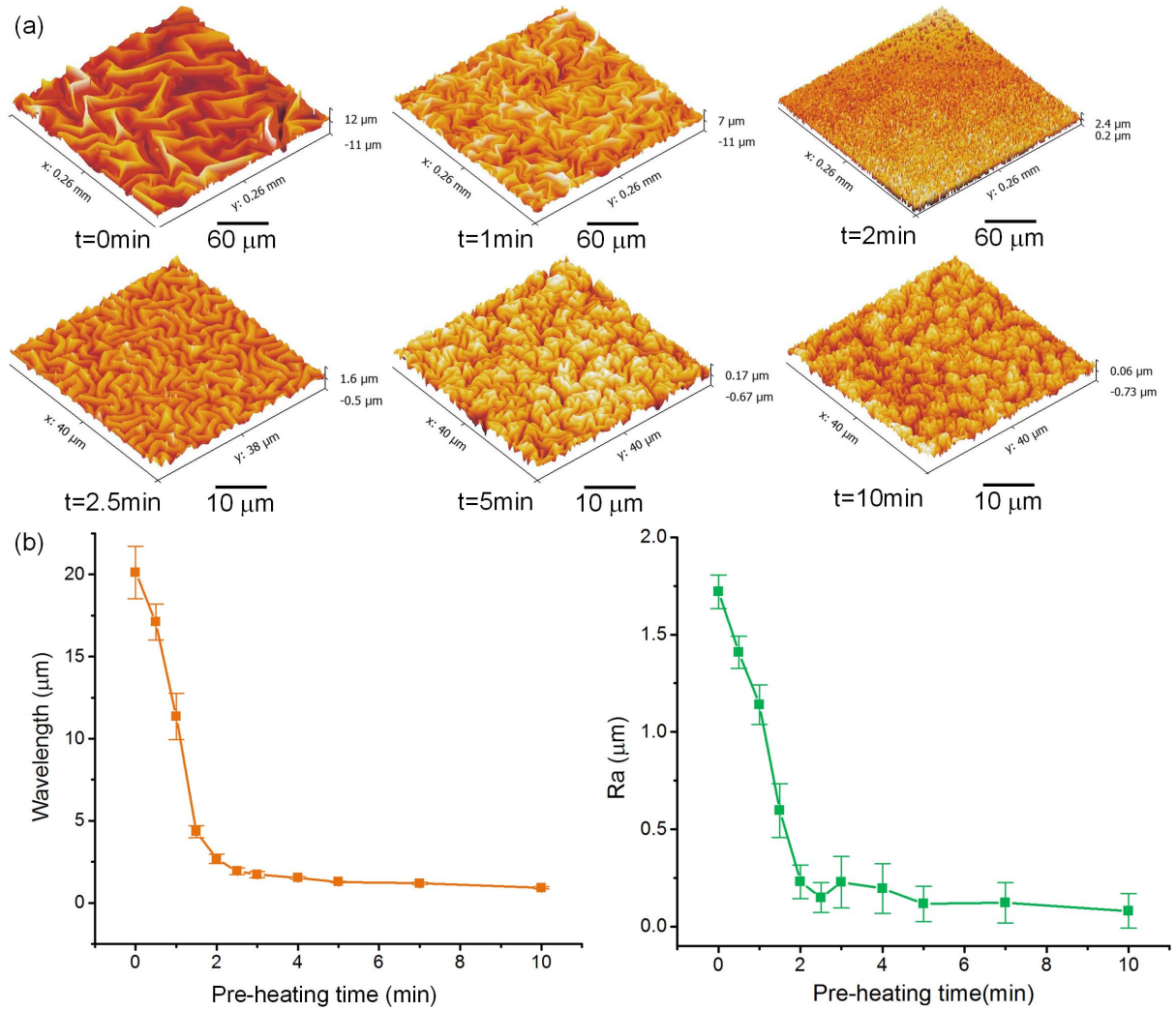


Fig. 3. (a) 3D images of wrinkle patterns with varying pre-heating time. (b) The wrinkle wavelength and Roughness as functions of pre-heating time.

wrinkle patterns were carried out using AFM for pattern  $\lambda < 2 \mu\text{m}$  and OLS for pattern  $\lambda > 2 \mu\text{m}$ , respectively. Fig. 3a shown the 3D images for wrinkle patterns with  $t$  from 0 min to 10 min. From these results we could observe the significant change in vertical scale of wrinkle patterns (i.e. the amplitude of wrinkle pattern) from tens micrometer to hundredes nanometers. Fig. 3b complies the results for plasma-induced wrinkling  $\lambda$  and the surface roughness ( $R_a$ ) as the function of pre-heating time  $t$ . As the increasing of heating time, the pattern  $\lambda$  decreased from 20.13  $\mu\text{m}$  to 0.92  $\mu\text{m}$  by 95.43%, and the largest pattern  $\lambda$  was 21.88 times of the smallest, which made it possible to obtain wrinkle pattern wavelength in a large range by simply controlling the pre-heating time. At the same time,  $R_a$  decreased from 1.60  $\mu\text{m}$  to 0.07  $\mu\text{m}$  by 95.63 % during  $t$  from 0 min to 10 min.

### B. Theoretical Analysis

The wrinkling phenomenon is usually treated as a simple stress model. In the region of low deformation, assuming a homogeneous film and bulk materials having perfect adhesion at the interface, wrinkle  $\lambda$  and amplitude  $A$  can be described

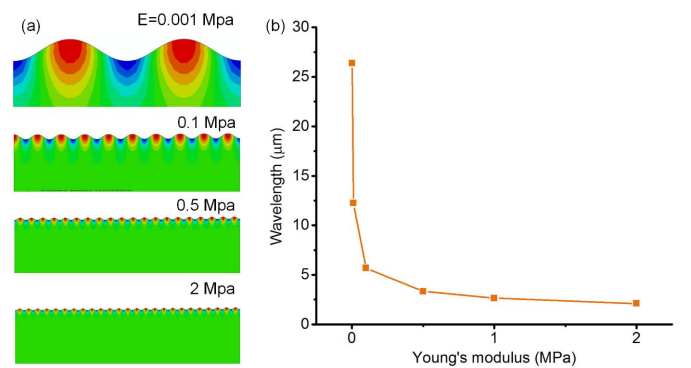


Fig. 4. Simulated results for the wrinkle pattern wavelength with different modulus of substrate.

by [2]:

$$\lambda = 2\pi h \left[ \frac{E_f(1 - \nu_s^2)}{3E_s(1 - \nu_f^2)} \right]^{1/3} \quad (1)$$

$$A = h \left( \frac{\varepsilon}{\varepsilon_c} \right)^{1/2} \propto R_a \quad (2)$$

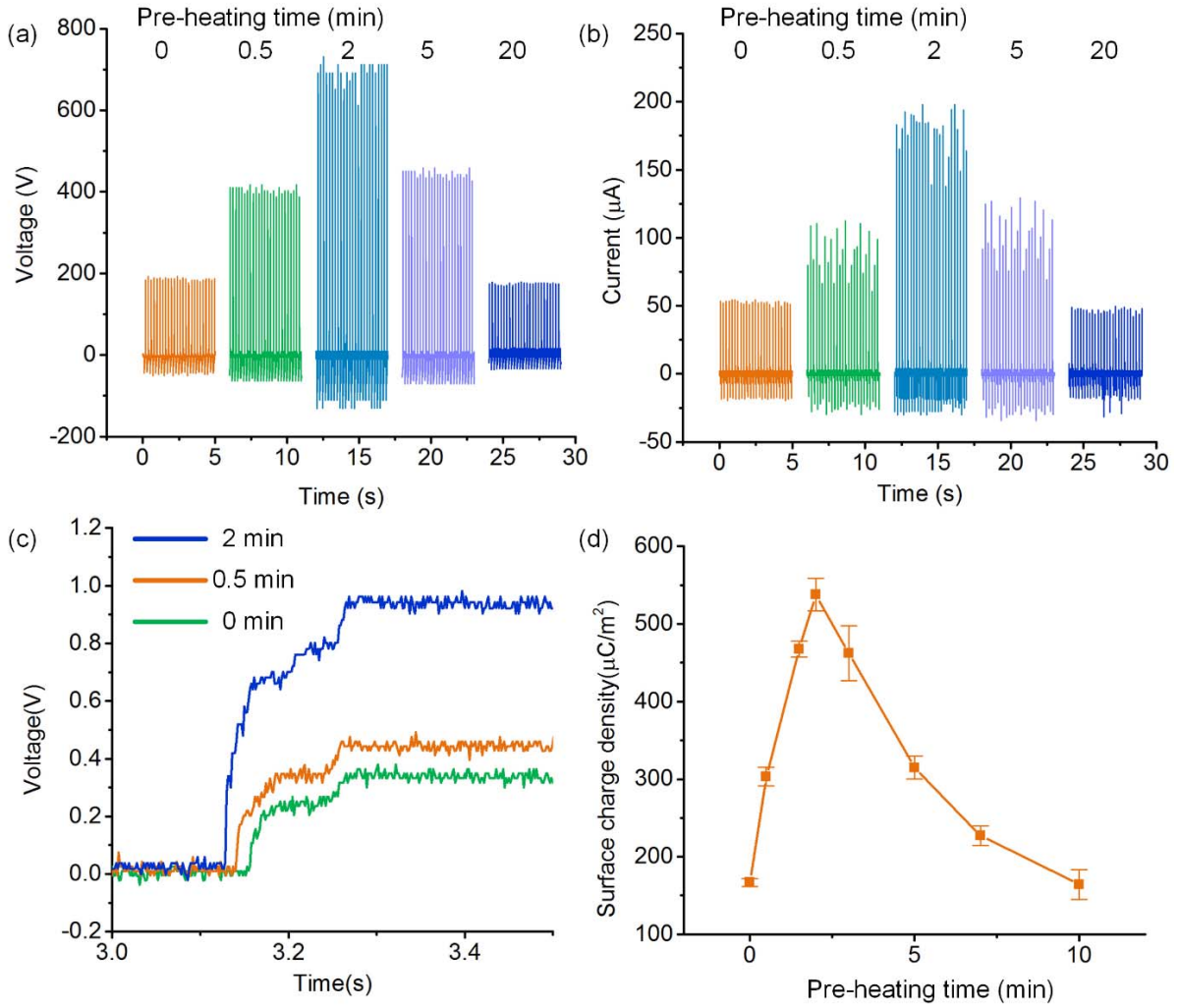


Fig. 5. Experiments for TENGs using the wide-range wrinkle patterns. (a) Voltage waveforms of TENGs using different pre-heating time wrinkle pattern. (b) Current waveforms of TENGs using different pre-heating time wrinkle pattern. (c) Charging curves for a  $1 \mu\text{F}$  capacitor of TENGs using different pre-heating time wrinkle pattern. (d) Calculated surface charge density of TENGs as a function of pre-heating time.

Where  $E$  is the elastic modulus,  $\varepsilon$  is the compressive strain,  $h$  and  $\nu$  represent the thickness of the stiff layer and Poisson ratio, the subscripts  $f$  and  $s$  denote the stiff film and the soft substrate, respectively,  $\varepsilon_c = \frac{1}{4} \left[ \frac{3E_s(1-\nu_f^2)}{E_f(1-\nu_s^2)} \right]^{1/3}$  is a critical strain, which must be exceeded to induce instability. Combined equation 2 and expression for  $\varepsilon_c$ , we can conclude that  $A \propto \lambda \sqrt{\varepsilon} \propto R_d$ . Considering that the mechanical parameters and thickness of the films are constant at the same plasma treating time, the pattern  $\lambda$  is inversely proportional to the substrate elastic modulus as  $\lambda \propto E_s^{-1/3}$ . Meanwhile, the elastic modulus of the PDMS is proportional to the cross-linking degree, which increases obviously with the pre-heating time  $t$ . Therefore, the pattern  $\lambda$  decreases steadily with the increasing of heating time, which also leads to surface roughness  $R_d$  inversely proportional to the heating time  $t$ .

To validate the influence of elastic modulus to wrinkle  $\lambda$ , we further simulated this phenomenon by finite element method using ABAQUS software. In this simulation, a constant uniaxial compressive displacement was applied to the right side

of PDMS substrate to simulate the compressive strain in our experiment, which was kept as 5% of the total length of PDMS substrate. By varying the elastic modulus ( $E$ ) of PDMS substrate, the simulated results are shown in Fig. 4a. It is obvious that the wrinkle  $\lambda$  decreased dramatically during  $E$  from 0.001 Mpa to 2 Mpa. Fig. 4b gave the simulated wrinkle wavelength as a function of Young's modulus of PDMS, which had a similar trend with our experimental results in Fig. 3b.

### C. Maximizing Surface Charge Density of a Triboelectric Nanogenerator

Here, at the aid of the pre-heating method, we fabricated arch-shaped TENGs using samples by pre-heating time from 0 min to 10 min, which have a size of  $3 \text{ cm} \times 3 \text{ cm}$  and a fixed maximum gap distance of about 3 mm.

The electric performance for these devices are summarized in Fig. 5. By increasing the pre-heating time  $t$ , the output voltage firstly had an increasing trend during  $t$  from 0 to 2 min as plotted in Fig. 5a. When the pre-heating time was longer than 2 min, the output voltage decreased with  $t$ . By varying the

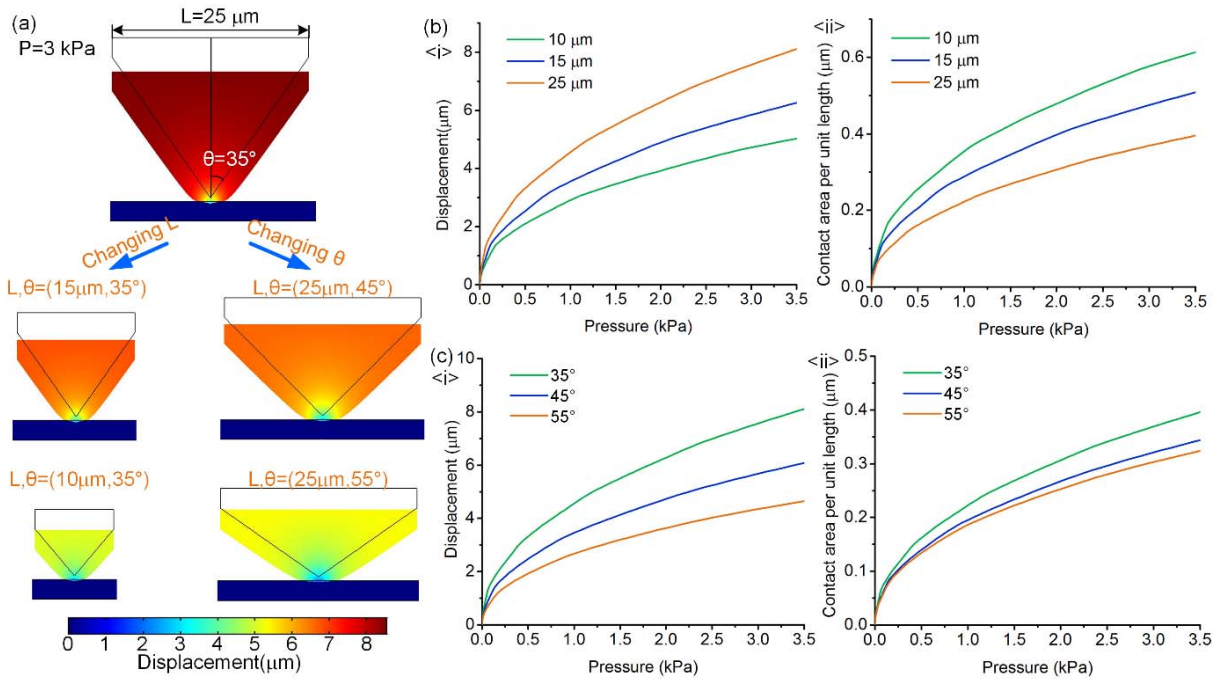


Fig. 6. (a) FEM simulated displacements of triangle structures with different parameters under 3 kPa pressure. (b) The displacement and contact area per unit length as functions as applied pressure and base line length of triangle. (c) The displacement and contact area per unit length as functions as applied pressure and  $\theta$ .

pre-heating time, the peak value of output voltage increased from 192 V to 685 V by 256 %. Fig. 5b shown the waveforms of output current from as-fabricated devices with different pre-heating time, which had a similar trend with the output voltage. A maximized value of nearly  $165\ \mu\text{A}$  was obtained at a pre-heating time of 2 min, which was increased by 201 % compared with TENG by 0 min pre-heated. The charging ability of these TENGs are measured by charging a  $1\ \mu\text{F}$  capacitor under finger typing through a full-wave rectifier as plotted in Fig. 5c. For the TENG using 0 min pre-heated sample, it can charge this capacitor to 0.35 V in single operational cycle, while the device using 2 min pre-heated membrane can charge this capacitor to 0.96 V, which was increased by 174 %. The inducted surface charge density of TENG is the ratio of charge amount transferred in a half operational cycle of TENG, which played dominated role in determining the TENG's electric performance. The inducted surface charge density  $\sigma_i$  of a TENG can be calculated by  $\sigma_i = V_C C / 2S$ , where  $V_C$ ,  $C$  are the voltage and value of the capacitor charged by a TENG in an operational cycle,  $S$  is the total area of a TENG. Usually, a relative large capacitor compared with the intrinsic capacitance of a TENG is need to obtain an appropriate value of the transferred charge under short-circuit [20]. Fig. 5d compiled the results of inducted surface charge density of TENGs as a function of pre-heating time. When  $t = 2$  min, a maximum surface charge density of  $537.6\ \mu\text{C}/\text{m}^2$  was observed, which was about 3.23 times of the untreated device. To the best of our knowledge, this value is the highest record of surface charge density of TENGs achieved in the published work, when taking the maximum force ( $\sim 50$  N) applied to the device into account.

#### D. Mechanism for the Improvement in the Electric Performance of TENG

Surface micro/nano pattern is one of the most used methods in improving the electric performance of TENG. Once adopting patterned surface as contact surface of TENG, the total surface area of TENG is expanded, and the effective contact area of TENG would increase with the outer force, leading to more charges accumulate on the contact surface and higher electric performance [32]. To further investigate and explain the mechanism of the outstanding ability of pre-heated wrinkle structure in improving the electric performance of TENG, finite element method with COMSOL software was employed to analyze the relationship between different scale wrinkle and outer force. The cross section of wrinkle structure is similar with sinusoidal shape curve. To simplify the calculation of contact area of the structure under pressure, two-dimensional triangle array was utilized in this simulation as plotted in Fig. 1 in supplementary material, which has two advantages: (1) the total surface area keeps the same during varying the scale of triangle when  $\theta$  is fixed; (2) the total surface area is inversly proportional to  $\theta$ , making it easier to vary the surface area by  $\theta$ .

Supposing the surface charge density  $\sigma$  produced by contact-electrification during contact-separation process is constant, the electric performance of TENG would be determined and increased linearly with the contact area. Benefited by the advantages mentioned above, we can individually simulate and calculate the influences of structure size and surface area by adjusting the base line length  $L_t$  of a triangle and  $\theta$  shown in Fig. 6a, respectively. Obviously, the displacements of triangles reduced with the decreasing of  $L_t$  and the

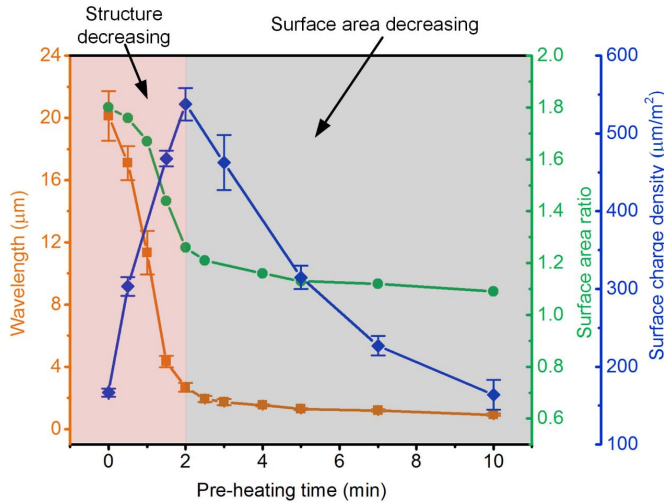


Fig. 7. The wrinkle wavelength surface area ratio and surface charge density of TENG as function of pre-heating time to imply reason for the two-section relationship with pre-heating time.

increasing of  $\theta$  at a pressure of 3 kPa. The contact area of single triangle corresponding to contact length  $L$  in two-dimensiona condition can be calculated by  $L = L_1 + L_2 = 2d/\sin\theta$ , where  $d$  is the displacement of triangle under pressure as illustrated in Fig. 1 in supplementary material. Fig. 6b plotted the influence of triangle size to the displacement of triangle and contact length. Under a specific pressure, the displacement increased with  $L_t$  during  $L_t$  from 10  $\mu\text{m}$  to 25  $\mu\text{m}$ . The contact area per unit length ( $L_u = L/L_t$ ) shown opposite trend and decreased with  $L_t$ . This means the contact area increases with the decreasing of  $L_t$ , which leads to higher electric performance. When varying  $\theta$ , both the displacement and contact area per unit length increased with the decrease of  $\theta$ , corresponding to higher electric performance. From this simulation, we can conclude: (1) when the total surface areas of TENGs are equal, TENGs with smaller structure would have higher electric performance under the same pressure; (2) when the structure scales of TENGs are comparable, the electric performance under the same pressure of a device with smaller surface area would be lower.

Thereby, the relationship between the electric performance of TENGs and wrinkle structures can be divided into two region: (1) stucture decreasing region, where wrinkle  $\lambda$  decreased dramatically from 20.13  $\mu\text{m}$  to 2.68  $\mu\text{m}$  as shown in Fig. 7, which generated the obviously improvement in electric performance of TENG; (2) surface area decreasing region, the surface area ratio decreased from 1.26 to 1.09 and accounts for the decreasing of surface charge density after 2 min. The surface area decreasing played a dominant role in this process and led to decrease of electric performance.

#### IV. CONCLUSIONS

In summary, a simple fabrication process based on pre-heating uncured PDMS and  $\text{C}_4\text{F}_8$  plasma treatment method is proposed to form wide-range controllable wrinkle structure. During the pre-heating process, the modulus of uncured PDMS increased with the pre-heating time, leading to the decrease

of wrinkle pattern  $\lambda$ , which was further proved by simulated results. Quantitatively characterization of the wrinkle pattern shown the pattern  $\lambda$  can be controlled from more than 20  $\mu\text{m}$  to lower than 1  $\mu\text{m}$ , decreased by more than 95%. Using the fabricated membrane with wrinkle pattern as contact pair of TENG, the electric performance of TENG was dramatically improved. A maximum surface charge density of 537.6  $\mu\text{C}/\text{m}^2$  was observed at a pre-heating time of 2 min. FEM simulation results implied the advantage of smaller scale structure with same surface area in improving the electric performance of TENG under relative low pressure region, which accounted for the influence of the wide-range wrinkle pattern to the performance of TENG. Our work provided a wide-range, simple, cost-effective and large area surface pattern methods for wrinkle morphologies fabrication, and demonstrated its strong ability in increase the electric performance for TENG, which could possibly speed up the application of wrinkle patterns as well as TENGs.

#### REFERENCES

- [1] J. Genzer and J. Groenewold, "Soft matter with hard skin: From skin wrinkles to templating and material characterization," *Soft Matter*, vol. 2, no. 4, pp. 310–323, 2006.
- [2] S. Yang, K. Khare, and P.-C. Lin, "Harnessing surface wrinkle patterns in soft matter," *Adv. Funct. Mater.*, vol. 20, no. 16, pp. 2550–2564, 2010.
- [3] E. P. Chan and A. J. Crosby, "Fabricating microlens arrays by surface wrinkling," *Adv. Mater.*, vol. 18, no. 24, pp. 3238–3242, 2006.
- [4] M. Melzer, G. Lin, D. Makarov, and O. G. Schmidt, "Stretchable spin valves on elastomer membranes by predetermined periodic fracture and random wrinkling," *Adv. Mater.*, vol. 24, no. 48, pp. 6468–6472, 2012.
- [5] K. Khare, J. Zhou, and S. Yang, "Tunable open-channel microfluidics on soft poly(dimethylsiloxane) (PDMS) substrates with sinusoidal grooves," *Langmuir*, vol. 25, no. 21, pp. 12794–12799, 2009.
- [6] Y. Rahmawan, C.-M. Chen, and S. Yang, "Recent advances in wrinkle-based dry adhesion," *Soft Matter*, vol. 10, no. 28, pp. 5028–5039, 2014.
- [7] W.-K. Lee, W.-B. Jung, S. R. Nagel, and T. W. Odom, "Stretchable superhydrophobicity from monolithic, three-dimensional hierarchical wrinkles," *Nano Lett.*, vol. 16, no. 6, pp. 3774–3779, 2016.
- [8] N. Gao, X. Zhang, S. Liao, H. Jia, and Y. Wang, "Polymer swelling induced conductive wrinkles for an ultrasensitive pressure sensor," *ACS Macro Lett.*, vol. 5, no. 7, pp. 823–827, 2016.
- [9] K. Efimenko, M. Rackaitis, E. Manias, A. Vaziri, L. Mahadevan, and J. Genzer, "Nested self-similar wrinkling patterns in skins," *Nature Mater.*, vol. 4, no. 4, pp. 293–297, 2005.
- [10] J.-Y. Park *et al.*, "Controlled wavelength reduction in surface wrinkling of poly(dimethylsiloxane)," *Soft Matter*, vol. 6, no. 3, pp. 677–684, 2010.
- [11] Y. Xuan *et al.*, "Crack-free controlled wrinkling of a bilayer film with a gradient interface," *Soft Matter*, vol. 8, no. 37, pp. 9603–9609, 2012.
- [12] F.-R. Fan, L. Lin, G. Zhu, W. Wu, R. Zhang, and Z. L. Wang, "Transparent triboelectric nanogenerators and self-powered pressure sensors based on micropatterned plastic films," *Nano Lett.*, vol. 12, no. 6, pp. 3109–3114, 2012.
- [13] Z. L. Wang, "Triboelectric nanogenerators as new energy technology for self-powered systems and as active mechanical and chemical sensors," *ACS Nano*, vol. 7, no. 11, pp. 9533–9557, 2013.
- [14] X.-S. Zhang, J. Brugger, and B. Kim, "A silk-fibroin-based transparent triboelectric generator suitable for autonomous sensor network," *Nano Energy*, vol. 20, pp. 37–47, Feb. 2016.
- [15] X. Chen *et al.*, "A wave-shaped hybrid piezoelectric and triboelectric nanogenerator based on P(VDF-TrFE) nanofibers," *Nanoscale*, vol. 9, no. 3, pp. 1263–1270, 2017.
- [16] X.-S. Zhang, M. Su, J. Brugger, and B. Kim, "Pencil-ing a triboelectric nanogenerator on paper for autonomous power MEMS applications," *Nano Energy*, vol. 33, pp. 393–401, Mar. 2017.
- [17] J. Chen *et al.*, "Networks of triboelectric nanogenerators for harvesting water wave energy: A potential approach toward blue energy," *ACS Nano*, vol. 9, no. 3, pp. 3324–3331, 2015.
- [18] J. Bae *et al.*, "Flutter-driven triboelectrification for harvesting wind energy," *Nature Commun.*, vol. 5, 2014, Art. no. 4929.

- [19] X. Cheng *et al.*, "A flexible large-area triboelectric generator by low-cost roll-to-roll process for location-based monitoring," *Sens. Actuators A, Phys.*, vol. 247, pp. 206–214, Aug. 2016.
- [20] Y. Ma *et al.*, "Self-powered, one-stop, and multifunctional implantable triboelectric active sensor for real-time biomedical monitoring," *Nano Lett.*, vol. 16, no. 10, pp. 6042–6051, 2016.
- [21] S. Niu *et al.*, "Theoretical study of contact-mode triboelectric nanogenerators as an effective power source," *Energy Environ. Sci.*, vol. 6, no. 12, pp. 3576–3583, 2013.
- [22] S. Wang, L. Lin, and Z. L. Wang, "Nanoscale triboelectric-effect-enabled energy conversion for sustainably powering portable electronics," *Nano Lett.*, vol. 12, no. 12, pp. 6339–6346, 2012.
- [23] Y. H. Kwon, S.-H. Shin, J.-Y. Jung, and J. Nah, "Scalable and enhanced triboelectric output power generation by surface functionalized nanointerprint patterns," *Nanotechnology*, vol. 27, no. 20, p. 205401, 2016.
- [24] X.-S. Zhang *et al.*, "High-performance triboelectric nanogenerator with enhanced energy density based on single-step fluorocarbon plasma treatment," *Nano Energy*, vol. 4, pp. 123–131, Mar. 2014.
- [25] L. Liu, W. Tang, and Z. L. Wang, "Inductively-coupled-plasma-induced electret enhancement for triboelectric nanogenerators," *Nanotechnology*, vol. 28, no. 3, p. 035405, 2016.
- [26] G. Zhu *et al.*, "Toward large-scale energy harvesting by a nanoparticle-enhanced triboelectric nanogenerator," *Nano Lett.*, vol. 13, no. 2, pp. 847–853, 2013.
- [27] S. Wang *et al.*, "Maximum surface charge density for triboelectric nanogenerators achieved by ionized-air injection: Methodology and theoretical understanding," *Adv. Mater.*, vol. 26, no. 39, pp. 6720–6728, 2014.
- [28] W. Tang *et al.*, "Liquid-metal electrode for high-performance triboelectric nanogenerator at an instantaneous energy conversion efficiency of 70.6%," *Adv. Funct. Mater.*, vol. 25, no. 24, pp. 3718–3725, 2015.
- [29] X. Cheng *et al.*, "Single-step fluorocarbon plasma treatment-induced wrinkle structure for high-performance triboelectric nanogenerator," *Small*, vol. 12, no. 2, pp. 229–236, 2015.
- [30] X. Cheng *et al.*, "A flexible and wearable generator with fluorocarbon plasma induced wrinkle structure," in *Proc. IEEE 29th Int. Conf. Micro Electro Mech. Syst. (MEMS)*, Jan. 2016, pp. 1181–1184.
- [31] X. Cheng *et al.*, "Controlled fabrication of nanoscale wrinkle structure by fluorocarbon plasma for highly transparent triboelectric nanogenerator," *Microsyst. Nanoeng.*, vol. 3, Jan. 2017, Art. no. 16074.
- [32] J. H. Lee, I. Yu, S. Hyun, J. K. Kim, and U. Jeong, "Remarkable increase in triboelectrification by enhancing the conformable contact and adhesion energy with a film-covered pillar structure," *Nano Energy*, vol. 34, pp. 233–241, Apr. 2017.



**Xiaoliang Cheng** received the B.S. degree from the University of Electronic Science and Technology, Chengdu, China, in 2014. He is currently pursuing the Ph.D. degree with the National Key Laboratory of Nano/Micro Fabrication Technology, Peking University, Beijing, China. His research interests mainly include design and fabrication of nanogenerator and mechanical energy harvester.



**Zijian Song** received the Ph.D. degree from the Beijing University of Aeronautics and Astronautics, Beijing, China, in 2015. He is currently involved in research as a Post-Doctoral Fellow with the National Key Laboratory of Nano/Micro Fabrication Technology, Peking University, Beijing. His research interests mainly include design and fabrication of nanogenerator and mechanical energy harvester, and MEMS and wearable device.



**Liming Miao** received the B.S. degree from Peking University, Beijing, in 2017. His research interests mainly include wrinkle structure and triboelectric nanogenerator.



**Zongming Su** received the B.S. degree from the University of Science and Technology, Beijing, in 2013. He is currently pursuing the Ph.D. degree with the National Key Laboratory of Nano/Micro Fabrication Technology, Peking University, Beijing, China. His research interests are micro and nano structure fabrication and energy harvesting.



**Yu Song** received the B.S. degree in electronic science and technology from the Huazhong University of Science and Technology, China, in 2015. He is currently pursuing the Ph.D. degree with the National Key Laboratory of Nano/Micro Fabrication Technology, Peking University, Beijing, China. He majors in MEMS, and his research is focusing on supercapacitors and self-charging power system.



**Hai-Xia (Alice) Zhang** (SM'10) received the Ph.D. degree in mechanical engineering from the Huazhong University of Science and Technology, Wuhan, China, in 1998. She is currently a Professor with the Institute of Microelectronics, Peking University, Beijing, China. Her research interests include MEMS design, fabrication technology, and micro energy technology. She has served as the Organizing Chair of Transducers'11 and the General Chair of IEEE NEMS 2013. As the Founder of the iCAN Contest, she has been organizing this worldwide event since 2007. In 2006, she received the National Invention Award of Science and Technology.